ACS Photonics

Article

pubs.acs.org/journal/apchd5

Helical Plasmonic Nanostructures as Prototypical Chiral Near-Field Sources

Martin Schäferling,*[,†] Xinghui Yin,[†] Nader Engheta,[‡] and Harald Giessen[†]

[†]4th Physics Institute, Research Center SCoPE, and Research Center SimTech, University of Stuttgart, Stuttgart, Germany

[‡]Department of Electrical and Systems Engineering, University of Pennsylvania, Philadelphia, Pennsylvania, United States

ABSTRACT: Plasmonic nanostructures can generate electromagnetic fields with high optical chirality that interact strongly with chiral molecules. We demonstrate how structures with chiral eigenmodes lead to chiral near-fields of predominantly one handedness. Our theoretical design with multiple metallic helices exhibits very high optical chirality over a large volume. The expected averaged chiroptical interaction is almost 2 orders of magnitude higher than for circularly polarized light.

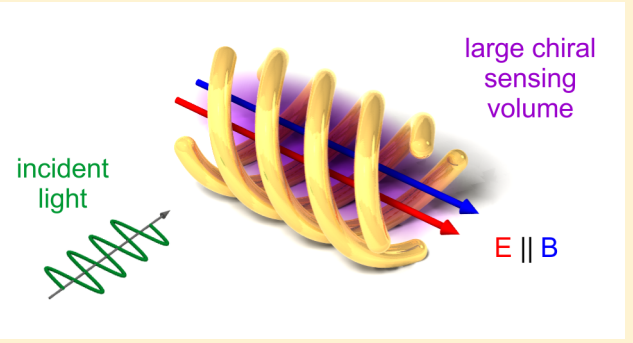

KEYWORDS: *optical chirality, plasmonics, near-field response, numerical simulation, circular dichroism, chiroptical spectroscopy*

Objects that cannot be superimposed with their mirror image are called chiral.[1] Chirality is a common concept in nature. Many biomolecules like, for example, the essential amino acids are chiral. This means that they exist in two enantiomeric forms that differ only in their handedness while all other physical properties are the same. Their chiral nature can only be probed by interactions with other chiral objects. One common method is the interaction with circularly polarized light that leads to a difference in the absorption depending on both the handedness of the molecule and that of the light.[2] However, this chiroptical response is small for most molecules, which renders such analysis rather challenging, especially when small volumes should be probed.[3,4]

Artificial chiral materials can show chiroptical responses that are several orders of magnitude stronger.[5] The three-dimensionality of these structures, which is an important prerequisite for chirality, could be obtained by stacking of planar structures[6−14] or by the combination of a planar structure with a substrate that breaks the symmetry.[15−18] Fully three-dimensional designs are possible by methods such as direct laser writing,[19,20] glancing angle deposition,[21,22] electron- and ion-beam induced deposition,[23,24] colloidal lithography with tilted angle evaporation,[25] or by a sophisticated method that utilizes the strain in heterostructured films.[26] Furthermore, self-assembly techniques have been used to fabricate a broad range of chiral plasmonic systems such as tetrahedral arrangements of differing nanoparticles[27−29] or chiral arrangements of similar building blocks.[30−33] Also, a broad understanding of the chiroptical far-field response of chiral plasmonic nanostructures has recently been gained.[34−45]

In the previous years, the potential of plasmonic structures for enhancing the chiroptical response of nearby chiral biomolecules has been analyzed both theoretically[46−49] and experimentally.[50−57] One approach uses the chiral near-field response of plasmonic nanostructures. The chiroptical interaction between an electromagnetic field and a chiral molecule can be described as[58,59]

$$A \propto \alpha_e U_e + \alpha_m U_b - \beta C \tag{1}$$

where A is the absorption of the molecule. U_e and U_b are the electric and magnetic energy density, respectively, while α_e and α_m are the imaginary parts of the corresponding electric and magnetic dipole polarizability. The so-called mixed electric-magnetic dipole polarizability β is a material parameter describing the intrinsic chirality of the molecule, while the optical chirality C is a chiral measure for the electromagnetic field. It can be calculated as[58,60]

$$C = -\frac{\varepsilon_0 \omega}{2} \mathrm{Im}(\mathbf{E}^* \cdot \mathbf{B}) \tag{2}$$

Here, **E** and **B** are the complex electric and magnetic fields. The optical chirality, which is connected to the helicity of the light,[61,62] quantifies the interaction strength of an electromagnetic field with a chiral molecule for a given β. The theoretical differential absorption for two enantiomeric fields, that is, $C^+ = -C^-$ and $U^+_{e,b} = U^-_{e,b}$, is directly proportional to the optical chirality. Maximum optical chirality in plane waves is obtained for circularly polarized light:

$$C^{\pm}_{\mathrm{CPL}} = \pm \frac{\varepsilon_0 \omega}{2c} |\mathbf{E}|^2 \tag{3}$$

Received: March 11, 2014
Published: May 12, 2014

The positive sign corresponds to left-handed, and the negative sign corresponds to right-handed circular polarization. Tang and Cohen demonstrated a measurement scheme where the electrical energy density is decreased while the optical chirality stays the same leading to an improved enantioselectivity.[63] Similar effects have been reported for light with orbital angular momentum.[64] Recent work has shown that also plasmonic nanostructures, whose geometry directly influences the properties of their near-fields, can be used to obtain chiral fields with strong optical chirality. Interestingly, although the combination of twisted structures with circularly polarized light can lead to chiral hot-spots,[65] even achiral structures illuminated with linearly polarized light can generate locally chiral near-fields.[48,66−68] First experiments confirmed these findings.[69]

However, many structures discussed in literature rely on the properties of the incident field. The designs discussed in ref 67 rely on circularly polarized light, while the concepts discussed in refs 48, 65, and 68 take the phase difference between incident and scattered fields into account, which might be sophisticated to control. Also, it is often not straightforward how to access only one handedness of the chiral fields. Many designs lead to both left- and right-handed near-fields that cancel each other on average.

In this paper, we introduce a novel concept: Plasmonic nanoantennas[70] that support chiral eigenmodes, meaning that the near-fields of the eigenmodes are chiral. By that means, the incident field is only necessary to excite those modes but has no further influence on the characteristics of the generated chiral near-fields. This reduces the parameters that must be controlled and may therefore lead to more reliable designs for the experiment. The overall chirality of the near-field should not vanish when integrating over the whole space to ensure that the structure and its generated chiral fields can be used without any additional requirements for applications such as enantiomer discrimination. Symmetry considerations dictate that structures that fulfill these conditions must be chiral themselves. Otherwise, parity inversion would change the net handedness of the near-field after averaging, but leave the structure itself unaltered.

RESULTS AND DISCUSSION

Equation 2 gives the condition for nonzero optical chirality: The electric and magnetic fields must have parallel components that are out of phase. A prototypical design that fulfills this condition is a helical structure, as shown in Figure 1. The fundamental mode has a dipolar character leading to an electric field vector pointing from one end to the other. A magnetic field in the same direction is generated due to the coiled wire. Also, the phase condition between electric and magnetic field is automatically fulfilled as the magnetic field scales with the current, while the electric field is maximum when the carriers are accumulated at the ends of the wire. Therefore, strong chiral near-fields are expected in the region surrounded by the wire. Changing the handedness of the helix will change the relative orientation of the two fields and therefore change the handedness of the respective near-fields.

As the fundamental mode of the helix by itself will generate chiral near-fields, the incident field is only needed to excite this mode. This can be carried out most efficiently by illuminating the helix from the top with linear polarization, as indicated in Figure 1. In this configuration, the external field couples to the dipole moment of the helix. Note that this scheme differs from

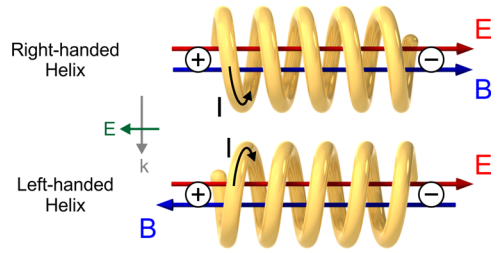

Figure 1. The fundamental mode of a helical plasmonic nanoantenna exhibits nonorthogonal electric and magnetic dipole moments. Within the structure, the electric (red) and magnetic (blue) field vectors are mainly parallel, leading to nonzero optical chirality. Changing the handedness of the structure flips the relative orientation of the field vectors and, therefore, the handedness of the chiral near-fields. Thus, such helical antennas are prototypes of a plasmonic nanostructure with strong chiral eigenmodes.

the usage of this structure as circular polarizer, where the helix is illuminated axially, that is, **k** is parallel to the axis of the helix. This illumination leads to different excitation for left- and right-handed circularly polarized light.[19,36]

The confinement of the chiral near-fields is best when the pitch of the helix is small. Figure 2a depicts the calculated

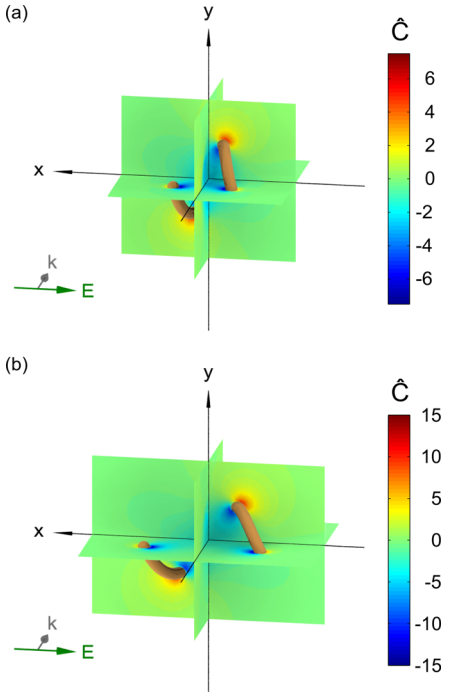

Figure 2. (a) A single helix with a small pitch exhibits well confined chiral near-fields. (b) The absolute values of optical chirality increase with increasing pitch, but the confinement becomes weaker.

normalized optical chirality $\hat{C}(\mathbf{r})$ near a small gold helix with a pitch of 50 nm excited at its fundamental resonance. The optical chirality of circularly polarized light has been used to perform the normalization:

$$\hat{C} := \frac{C}{C^{+}_{\mathrm{CPL}}} \tag{4}$$

The radius of the helix is 30 nm, and the wire diameter is 10 nm. The plot shows that nonzero optical chirality is not only found close to the metal, but also inside the helix, as expected.

dx.doi.org/10.1021/ph5000743 | ACS Photonics 2014, 1, 530−537

On the other hand, a larger pitch increases the dipole moment of the structure and therefore improves the coupling to the external field. This can lead to an increase of the absolute values of optical chirality, as seen in Figure 2b for a pitch of 100 nm, but with weaker confinement of the fields. The ultimate limit is a straight rod antenna, as discussed in ref 67. This leads to a trade-off between strength, confinement, and net chirality of the generated fields. An optimum design should feature strong chiral near-fields of one handedness over a large volume.

To obtain this goal, the initial design of a single helix must be extended. Figure 3 sketches two different approaches. The first

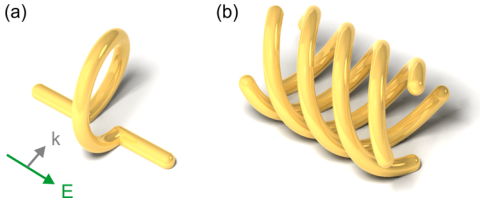

Figure 3. Modified designs that are expected to feature simultaneously strong chiral near-fields and good coupling to the external field. (a) The dipole moment of the loop-wire structure is enlarged due to the linear antennas at each side of the loop. (b) Designs with multiple helices couple well to the external field as the pitch of each single helix can be enlarged. Simultaneously, the wires surround a larger volume.

one (Figure 3a) starts from a helix with a small pitch and adds additional antennas at each end to increase the coupling to the external field. This so-called loop-wire structure has already been discussed as prototype for plasmonic structures with strong chiroptical far-field response,[71,72] but should also feature promising near-field characteristics. However, due to the small pitch, the volume covered by chiral near-fields is limited. Therefore, we will focus on the second approach sketched in Figure 3b: We start with a large pitch helix, which automatically leads to a larger volume that is enclosed by gold wires. To obtain a better confinement of the fields, additional helices are added. A similar approach has been also used for circular polarizers, where superstructures of multiple helices have been used to improve the circular polarization extinction ratio.[73−75]

Small Four-Helix Design. Additional helices lead to a more complicated behavior of the whole design as the single helices can interact with one another. Figure 4a shows the extinction cross section of four interlocking helices for pitch values varying from 50 to 150 nm. The pitch is varied by 10 nm for neighboring plots. All other dimensions are the same as for the single helix calculated in Figure 2. As expected, the extinction cross section increases with increasing pitch, as the structure couples stronger to the external field. However, for small pitch values an increase of the pitch leads to a blueshift of the fundamental resonance. This is in contrast to the expectation, as an increasing pitch leads to longer wires and should therefore result in a redshift. It can be explained by analyzing the mode hybridization in the four-helix structure. Only the lower energy mode is excited by the external dipolar field. This mode exhibits a strong blueshift when the coupling is reduced due to an enlargement of the pitch. In the case of small pitches, where the initial coupling is sufficiently strong, this blueshift can supersede the intrinsic redshift resulting from the elongation of the wires. The redshift dominates the observed behavior for pitches larger than 100 nm.

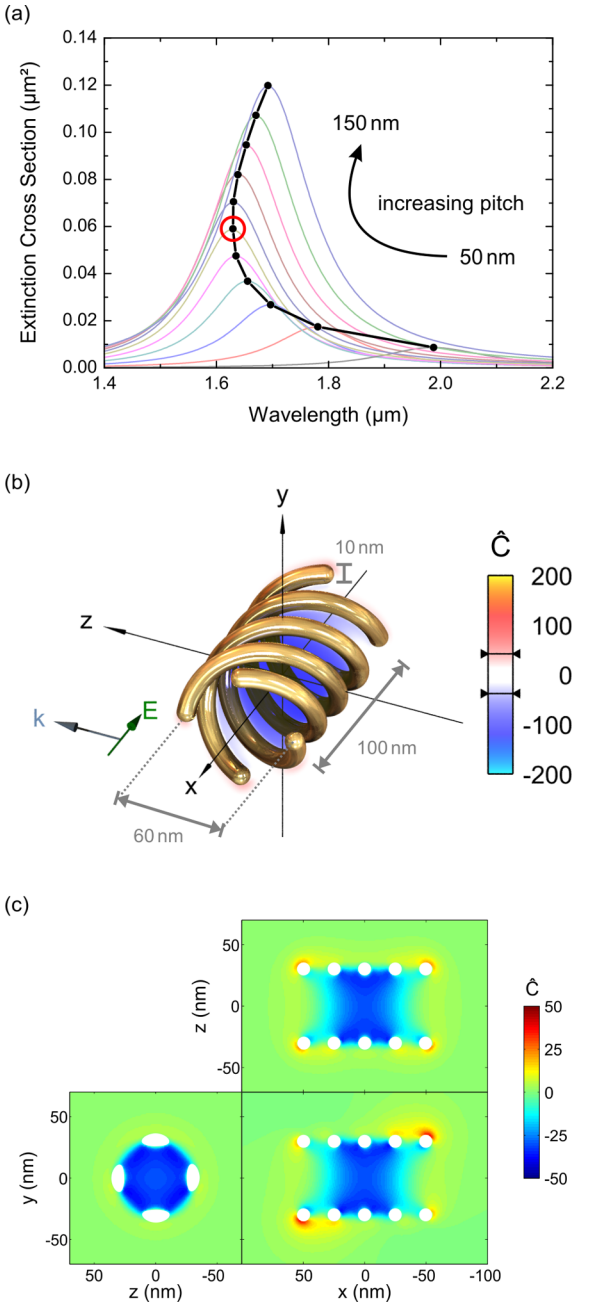

Figure 4. (a) The extinction cross section of the four-helix structure increases with increasing pitch. A strong blueshift occurs when starting from small pitch values. This switches to the expected redshift when the pitch is further increased. The pitch is changed by 10 nm for neighboring plots. (b) Strongly confined chiral near-fields are generated within the helices for a pitch of 100 nm (red circle in a). (c) The slice plots confirm the confinement to the interior region.

Figure 4b shows a three-dimensional map of the optical chirality around a four-helix structure with a pitch of 100 nm on resonance (red circle in Figure 4a). The resonance position is located in the near-infrared wavelength regime at 1.63 μm. The chiral near-fields are mainly located inside the structure and are enclosed by the wires. The slice plots in Figure 4c confirm this observation. Note that the fields are right-handed ($C < 0$) in the whole interior of the structure. Left-handed fields also occur (mainly at the ends of the wires), but when averaging over the whole volume, the right-handed characteristic of the near-fields

dx.doi.org/10.1021/ph5000743 | ACS Photonics 2014, 1, 530−537

dominates. This is in accordance with the right-handed nature of the structure.

The structure also performs well regarding the absolute values of normalized optical chirality. Maximum and minimum values are indicated by the horizontal bars in Figure 4a. This particular design reaches −38 for the minimum optical chirality. Higher values have been reported for other structures, but only in some hot spots.[65] The four-helix structure, on the other hand, features near-fields with significantly higher optical chirality than circularly polarized light of the same frequency over an extended volume.

When the pitch is further increased to 150 nm, the maximum and minimum values of optical chirality stay almost the same, although the extinction cross section roughly doubles. Additionally, the confinement of the fields becomes weaker as already discussed for the single helix. Therefore, we attribute the characteristics of the four-helix structure to the coupling between the single wires. Increasing the pitch further than 100 nm, where the resonance position starts to shift red with further increasing pitch, seems to have no benefit for the generation of chiral near-fields.

Note that the dimensions of the design are very small, which could pose challenges for fabrication. Recently, Mark and collaborators have fabricated single helices with comparable dimensions by a glancing angle deposition technique.[21] However, especially the ratio between helix diameter and wire thickness is substantially smaller than in our calculations, which leads to a narrowing of the accessible volume inside the helix. DNA nanoassembly with subsequent metal coating might offer an alternative route, but the DNA scaffolds prevent the analyte from reaching the interior region.[31] Helices with feature sizes below 100 nm have been fabricated by electron-beam induced deposition, but the metal is incorporated in a carbon matrix, which is expected to weaken the near-field response.[23] Additionally, all of these techniques have been used to fabricate only single helices thus far. The step to the suggested four-helix design seems to be nontrivial.

Large Four-Helix Design. A technique that could in principle fabricate the proposed design is 3D direct laser writing (DLW) as it is very versatile in terms of possible geometries. However, the laser wavelength limits the minimum feature size. Additionally, the smallest voxels that can be written are elliptical due to a difference between the axial and the longitudinal resolution. Recent developments such as STED DLW,[76] utilization of the diffusion of quencher molecules[77] or the combination of DLW with spatial light modulators[78] significantly improved both the resolution as well as the voxel aspect ratio. However, the dimensions of the small design discussed in the previous chapter are still out of reach for DLW with present techniques.

Therefore, we now analyze the behavior of a 20 times larger version of our four-helix design. Now, the pitch of the structure is 2.0 μm, the helix radius is 0.6 μm, and the diameter of the wire is 0.2 μm. Such dimensions are in principle feasible for a 3D direct laser writing approach. However, the obtained optical chirality is reduced by a factor of roughly 1.7 compared to the original design (cf., Figure 5). The scales of both the three-dimensional map and the slice plots are the same as in Figure 4 that showed the small version of the design. This is even more striking as the dipole moment of the structure is strongly increased due to the upscaling. Therefore, higher values of optical chirality were expected.

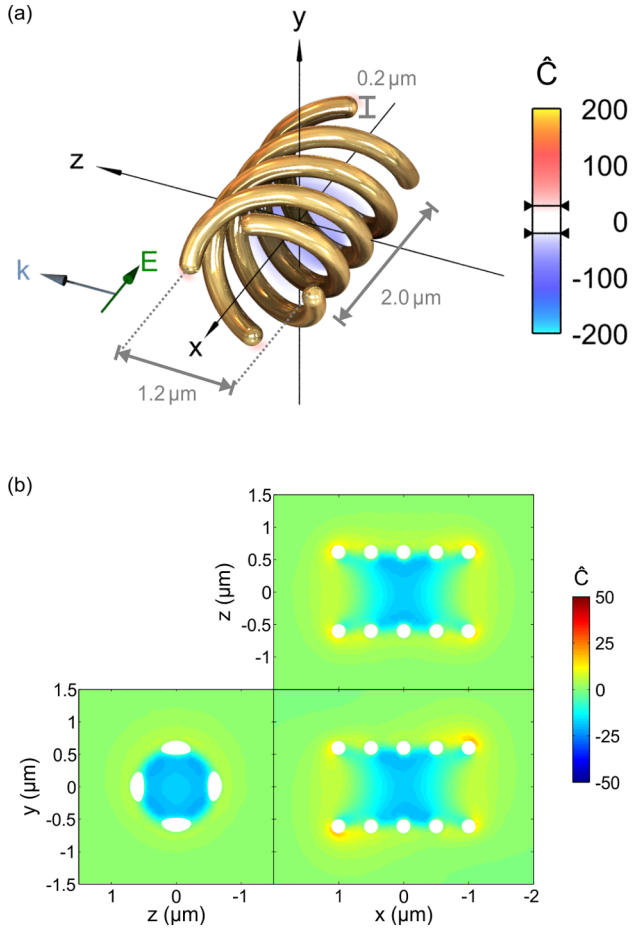

Figure 5. (a) The optimum design is enlarged by a factor of 20 to enable fabrication by 3D direct laser writing. After this upscaling process, the obtained normalized optical chirality is decreased. (b) The slice plots demonstrate a drop by a factor of 1.7 compared to the small design.

We also calculated the far-field response depending on the pitch as already done for the small four-helix structure to obtain further insight in the behavior of the enlarged design. The results are shown in Figure 6a for pitch values between 1.0 and 2.0 μm. Neighboring plots differ by 0.1 μm in pitch. As for the smaller structure, these values are in the range where we obtain a blueshift when increasing the pitch. Also, the extinction cross section increases with the structure, as expected. Interestingly, the absorption cross section behaves differently for the enlarged structure. One obtains a decreasing absorption cross section with increasing pitch. This behavior is opposite to the small four-helix structure where the absorption and scattering cross sections show the same scaling behavior.

Figure 6b depicts the normalized optical chirality around the large four-helix structure for the smallest pitch calculated (1.0 μm, red circle in Figure 6a). Compared to the 2.0 μm pitch, the optical chirality is enhanced by a factor of roughly 8. The resulting chiral near-fields reach values for the optical chirality down to −179, which even exceeds the best design of the small four-helix structure and is, to the best of our knowledge, the highest value reported in literature thus far. The slice plots (Figure 6c) confirm that we also obtain predominantly right-handed near-fields that are confined to the interior of the structure. Compared to the small four-helix design, the values decrease faster when we move away from the

dx.doi.org/10.1021/ph5000743 | ACS Photonics 2014, 1, 530−537

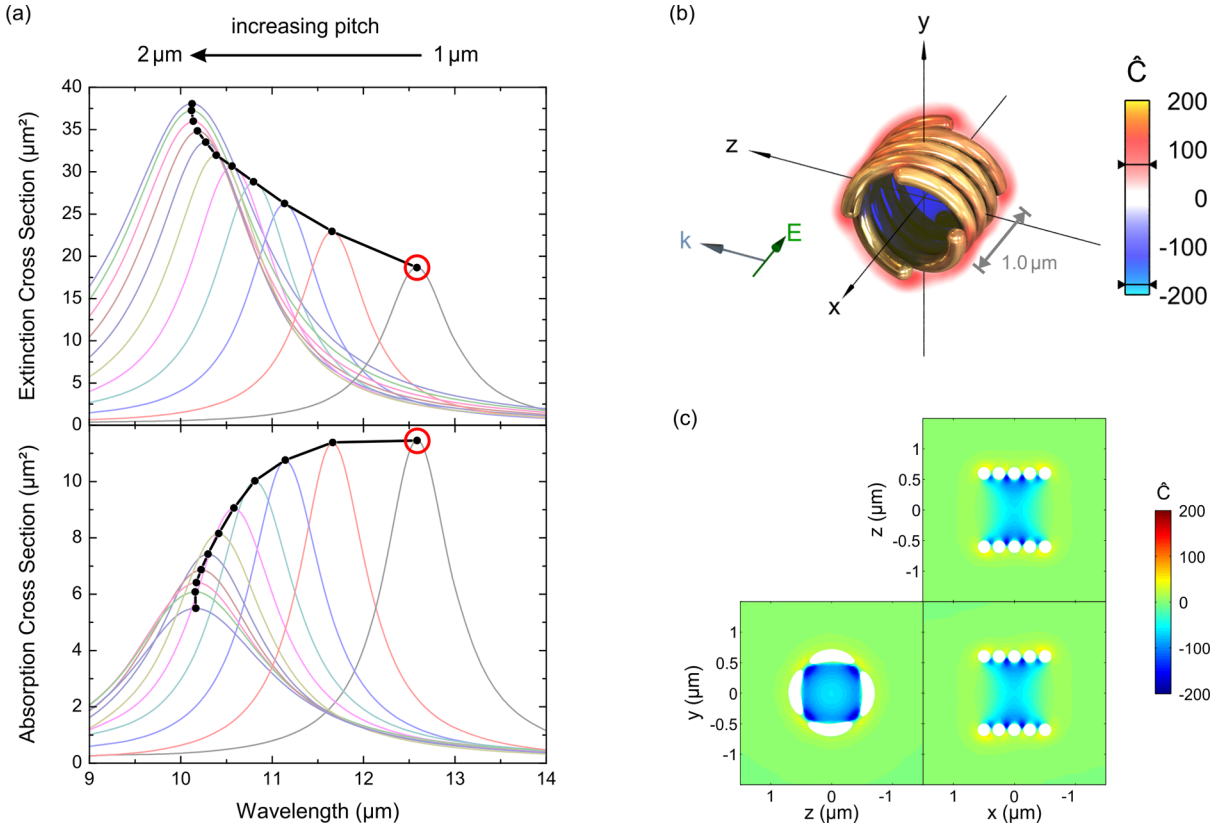

Figure 6. (a) Extinction and absorption cross section of the upscaled four-helix structure. The pitch is changed by 0.1 μm for neighboring plots. Maximum absorption is obtained for the smallest pitch (1.0 μm, red circle). (b) The three-dimensional optical chirality map for this pitch value shows strong chiral near-fields of one handedness in the whole interior of the nanostructure. (c) The slice plots confirm the confinement to the inner region.

wires toward the center of the structure. This can be explained by the stronger coupling between the wires in case of the enlarged structure with smaller pitch that leads to higher field enhancement in the gap and therefore higher values of optical chirality at the respective positions. Nevertheless, we still obtain substantial chiral near-fields in the center of the structure that exceed the response of the small four-helix structure. It is also noteworthy that a decrease of the pitch of the small design does not lead to the same effect. In the contrary, the optical chirality is weakened because the influence of the weaker coupling to the external field is stronger than the benefits from the stronger coupling between the wires in this case.

It should also be mentioned that this design is more difficult to fabricate because of the small gaps between the wires when compared to designs with larger pitch values. Additionally, the enlarged version shifts the operating wavelength to the mid infrared wavelength regime, which might be a drawback for some applications. The resonance frequency is very sensitive to the actual pitch due to the coupling between the wires, which is also challenging for fabrication. A balance between performance and fabrication demands should be found for real applications.

Of course, the details of this optimization depend crucially on the fabrication technique that is used. The chosen technique might also introduce additional imperfections such as grainy surfaces or deviations from the assumed perfectly round shape of the wires. The former influences the near-fields only very close to the surface;[79] the latter might modify the coupling between the helices. While our findings provide fundamental insights into the working principle and general characteristics of the proposed design, more specialized calculations are necessary for realistic modeling of definite experiments.

Additionally, the plasmonic resonance of the structure should be tuned to the chiroptical response of the target analyte to obtain strongest enhancement. Our designs exhibit their resonances in the near- to mid-infrared wavelength region. This is the region of fundamental vibrational circular dichroism modes.[80] Therefore, our design is best-suited to enhance this response, which is even smaller than standard circular dichroism occurring in the ultraviolet for most molecules. Smaller structures with plasmonic resonances in the visible have also the potential to enhance visible electronic circular dichroism.

When the four-helix design is used for chiroptical spectroscopy, it is not sufficient to only consider single spatial points. Rather, one obtains the response that is of interest by averaging over a specific volume that is filled with a chiral analyte. The recorded quantity in a circular dichroism type measurement is the difference in absorption for two electromagnetic fields of the same energy density with opposite handedness:

$$\Delta A = A^{-} - A^{+} \propto 2\beta C^{+} \tag{5}$$

where C^{+} corresponds to the optical chirality of the predominantly left-handed field. To obtain such field pairs, both enantiomers of the nanostructure can be used to create the respective fields. In this case, corresponding locations, where the near-fields are interchangeable by parity, can be found (cf., Supporting Information of ref 67). Then, the

dx.doi.org/10.1021/ph5000743 | ACS Photonics 2014, 1, 530−537

differential response of two molecules situated at these positions has the same form as eq 5.

We can now compare this response to the difference signal by a standard circular dichroism measurement, that is, with circularly polarized light. Using eq 3, we obtain

$$\Delta A_{CD} \propto \frac{\varepsilon_0 \omega}{c} \beta |\mathbf{E}|^2 \tag{6}$$

This leads to the difference signal enhancement of

$$\Delta \hat{A} := \frac{\Delta A}{\Delta A_{CD}} = \frac{C^+}{C^+_{CPL}} =: \hat{C}^+ \tag{7}$$

that yields a factor by which the response is expected to be enhanced due to the presence of the nanostructure (and the described measurement scheme) for every point in space compared to a circular dichroism measurement. Averaging over a specific volume V finally leads to

$$\langle \Delta \hat{A} \rangle_V := \frac{1}{V} \int_V \hat{C}^+ dV = -\frac{1}{V} \int_V \hat{C}_{helix} dV \tag{8}$$

which quantifies the expected enhancement of the response when V is filled with a chiral analyte. The negative sign has been added because the calculated fields $\hat{C}_{helix}$ for the different helical nanostructures analyzed are right-handed inside the structures and therefore show negative optical chirality.

We evaluated eq 8 for the large four-helix structure with a pitch of 1.0 that showed the strongest chiral near-fields. V has been chosen as volume of a cylinder with radius r and length L that is collinear with the helix. Figure 7 shows the value of

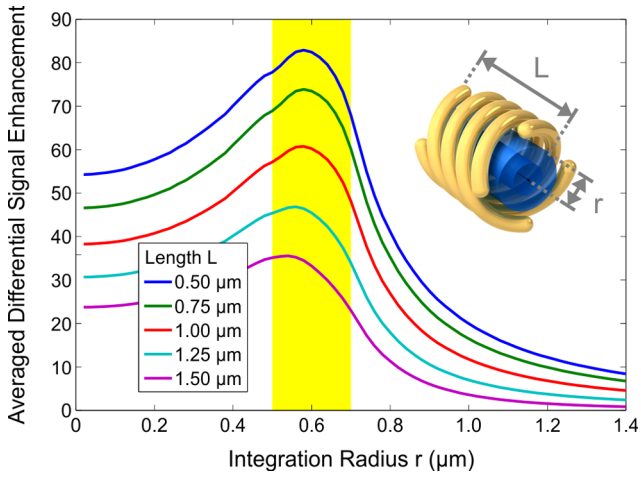

Figure 7. The averaged normalized optical chirality is a measure of the possible enhancement of chiroptical responses compared to a circular dichoism measurement when the integration area is filled with a chiral analyte. The integration has been performed for cylindrical areas with varying radius r (cf. inset). The results are plotted for several cylinder lengths L. All evaluations have been performed for the large four-helix structure with a pitch of 1.0 μm at its fundamental resonance (12.6 μm). The yellow stripe depicts the area where the gold wires are located.

$\langle \Delta \hat{A} \rangle_V$ depending on r. The different plots correspond to different lengths L. The yellow vertical area depicts the location of the wires. When r reaches this area, the integration volume penetrates into the metal. The respective points have been excluded from the volume calculation, as they cannot be accessed by the chiral analyte.

Significant enhancement of the response is expected for all values of L as long as the chiral analyte is restricted to the interior of the helix. As soon as the analyte also reaches the exterior parts, the signal drops. This is due to the increasing volume with chiral near-fields with opposite or vanishing optical chirality. As $\langle \Delta \hat{A} \rangle_V$ describes the enhancement compared to the whole volume beeing analyzed by circular dichroism spectroscopy, its value is obviously maximal when V is confined to the region with highest optical chirality. For an infinite radius, $\langle \Delta \hat{A} \rangle_V$ approaches zero. Small radii, on the other hand, also lower the response because the strongest chiral near-fields are located closer to the wires. Therefore, maximum signal enhancement is obtained when r equals the radius of the four-helix structure.

The optical chirality is longitudinally confined to the center of the structure: Larger values of L lead to a smaller overall chiral response. When L exceeds the pitch of the structure, the maximum enhancement shifts to lower radii as the exterior of the structure possesses near-fields with opposite optical chirality to its interior (cf., Figure 6c). Highest enhancement is obtained for small values of L. For a cylinder length that equals half of the pitch, enhancement factors of more than 80 have been calculated.

CONCLUSIONS

We have demonstrated that plasmonic nanostructures consisting of multiple helices generate near-fields with high optical chirality over an extended region. The incident field is only used to excite the resonance of the structure. The chiral eigenmodes lead to chiral near-fields of one handedness inside the structure. Depending on the dimensions of the helices, different approaches are necessary to maximize the obtained optical chirality: Small structures need a sufficiently large pitch to obtain good coupling to the external field, whereas large structures benefit from small pitches and the resulting stronger coupling between the single wires. We showed that these structures can be utilized as near-field sources for chiroptical spectroscopy with an almost 2 orders of magnitude enhanced response compared to circularly polarized light. By this means, our designs aid as prototypes for chiral near-field sources for applications such as optical enantiomer discrimination.

METHODS

Simulation. All simulations were performed by a third-order frequency domain solver (CST Microwave Studio) using a third-order tetrahedral mesh. The gold was modeled by a Drude model with a plasma frequency of 1.37×10^{16} s^{-1} and a collision frequency of 1.22×10^{14} s^{-1}. The helices were modeled as single structures in vacuum. Additional space was added until no influence from reflections at the open boundaries on the resulting values for optical chirality occurred. Additional adjustments on the parameters for the mesher were necessary to resolve the small helices properly. To suppress single numerical errors at the interfaces, the calculated optical chirality has been filtered by a $3 \times 3 \times 3$ median filter. For comparison, the optical chirality has been normalized by the optical chirality of circularly polarized light at the same frequency.

Visualization. The three-dimensional optical chirality maps were generated by POV-Ray. The volume rendering was obtained by a transparent medium whose density and color is determined by the local value of optical chirality. Due to the

dx.doi.org/10.1021/ph5000743 | ACS Photonics 2014, 1, 530−537

transparency the color of one distinct point depends not only on the actual optical chirality value at this point but also on the color of the region behind. Please refer to the two-dimensional slice plots to obtain quantitative insights. The three-dimensional maps should be only used to compare the response of different designs. All maps share the same colormap to support this purpose.

AUTHOR INFORMATION

Corresponding Author

*E-mail: m.schaeferling@pi4.uni-stuttgart.de.

Notes

The authors declare no competing financial interest.

ACKNOWLEDGMENTS

The authors thank Uday K. Chettiar for helpful discussions and Sven M. Hein for help with the visualization. Parts of this work have been financially supported by DFG, BMBF, Baden-Württemberg Stiftung, ERC (COMPLEXPLAS), and a MPI-FKF guest professorship for N.E. X.Y. additionally acknowledges support by the Carl-Zeiss foundation.

REFERENCES

(1) Kelvin, W. T. *Baltimore Lectures on Molecular Dynamics and the Wave Theory of Light*; CJ Clay and Sons: London, 1904.

(2) Engheta, N.; Jaggard, D. Electromagnetic chirality and its applications. *IEEE Antennas Propag. Soc. Newsl.* **1988**, *30*, 6−12.

(3) Berova, N., Nakanishi, K., Woody, R. W., Eds. *Circular Dichroism: Principles and Applications*, 2nd ed.; Wiley-VCH: New York, 2000.

(4) Barron, L. D. *Molecular Light Scattering and Optical Activity*, 2nd ed.; Cambridge University Press: New York, 2004.

(5) Valev, V. K.; Baumberg, J. J.; Sibilia, C.; Verbiest, T. Chirality and chiroptical effects in plasmonic nanostructures: fundamentals, recent progress, and outlook. *Adv. Mater.* **2013**, *25*, 2517−2534.

(6) Rogacheva, A. V.; Fedotov, V. A.; Schwanecke, A. S.; Zheludev, N. I. Giant gyrotropy due to electromagnetic-field coupling in a bilayered chiral structure. *Phys. Rev. Lett.* **2006**, *97*, 177401.

(7) Decker, M.; Klein, M. W.; Wegener, M.; Linden, S. Circular dichroism of planar chiral magnetic metamaterials. *Opt. Lett.* **2007**, *32*, 856−858.

(8) Decker, M.; Ruther, M.; Kriegler, C. E.; Zhou, J.; Soukoulis, C. M.; Linden, S.; Wegener, M. Strong optical activity from twisted-cross photonic metamaterials. *Opt. Lett.* **2009**, *34*, 2501−2503.

(9) Liu, N.; Liu, H.; Zhu, S.; Giessen, H. Stereometamaterials. *Nat. Photonics* **2009**, *3*, 157−162.

(10) Menzel, C.; Helgert, C.; Rockstuhl, C.; Kley, E.-B.; Tünnermann, A.; Pertsch, T.; Lederer, F. Asymmetric transmission of linearly polarized light at optical metamaterials. *Phys. Rev. Lett.* **2010**, *104*, 253902.

(11) Decker, M.; Zhao, R.; Soukoulis, C. M.; Linden, S.; Wegener, M. Twisted split-ring-resonator photonic metamaterial with huge optical activity. *Opt. Lett.* **2010**, *35*, 1593−1595.

(12) Helgert, C.; Pshenay-Severin, E.; Falkner, M.; Menzel, C.; Rockstuhl, C.; Kley, E. B.; Tuennermann, A.; Lederer, F.; Pertsch, T. Chiral metamaterial composed of three-dimensional plasmonic nanostructures. *Nano Lett.* **2011**, *11*, 4400−4404.

(13) Hentschel, M.; Schäferling, M.; Weiss, T.; Liu, N.; Giessen, H. Three-dimensional chiral plasmonic oligomers. *Nano Lett.* **2012**, *12*, 2542−2547.

(14) Zhao, Y.; Belkin, M. A.; Alù, A. Twisted optical metamaterials for planarized ultrathin broadband circular polarizers. *Nat. Commun.* **2012**, *3*, 870.

(15) Papakostas, A.; Potts, A.; Bagnall, D.; Prosvirnin, S.; Coles, H.; Zheludev, N. Optical manifestations of planar chirality. *Phys. Rev. Lett.* **2003**, *90*, 107404.

(16) Kuwata-Gonokami, M.; Saito, N.; Ino, Y.; Kauranen, M.; Jefimovs, K.; Vallius, T.; Turunen, J.; Svirko, Y. Giant optical activity in quasi-two-dimensional planar nanostructures. *Phys. Rev. Lett.* **2005**, *95*, 227401.

(17) Plum, E.; Liu, X.-X.; Fedotov, V.; Chen, Y.; Tsai, D.; Zheludev, N. Metamaterials: optical activity without chirality. *Phys. Rev. Lett.* **2009**, *102*, 113902.

(18) Valev, V. K.; Smisdom, N.; Silhanek, a. V.; De Clercq, B.; Gillijns, W.; Ameloot, M.; Moshchalkov, V. V.; Verbiest, T. Plasmonic ratchet wheels: switching circular dichroism by arranging chiral nanostructures. *Nano Lett.* **2009**, *9*, 3945−3948.

(19) Gansel, J. K.; Thiel, M.; Rill, M. S.; Decker, M.; Bade, K.; Saile, V.; von Freymann, G.; Linden, S.; Wegener, M. Gold helix photonic metamaterial as broadband circular polarizer. *Science* **2009**, *325*, 1513−1515.

(20) Radke, A.; Gissibl, T.; Klotzbücher, T.; Braun, P. V.; Giessen, H. Three-dimensional bi-chiral plasmonic crystals fabricated by direct laser writing and electroless silver plating. *Adv. Mater.* **2011**, *23*, 3018−3021.

(21) Mark, A. G.; Gibbs, J. G.; Lee, T.-C.; Fischer, P. Hybrid nanocolloids with programmed three-dimensional shape and material composition. *Nat. Mater.* **2013**, *12*, 802−807.

(22) Gibbs, J. G.; Mark, A. G.; Eslami, S.; Fischer, P. Plasmonic nanohelix metamaterials with tailorable giant circular dichroism. *Appl. Phys. Lett.* **2013**, *103*, 213101.

(23) Höflich, K.; Yang, R. B.; Berger, A.; Leuchs, G.; Christiansen, S. The direct writing of plasmonic gold nanostructures by electron-beam-induced deposition. *Adv. Mater.* **2011**, *23*, 2657−2661.

(24) Esposito, M.; Tasco, V.; Todisco, F.; Benedetti, A.; Sanvitto, D.; Passaseo, A. Three dimensional chiral metamaterial nanospirals in the visible range by vertically compensated focused ion beam induced-deposition. *Adv. Opt. Mater.* **2014**, *2*, 154−161.

(25) Frank, B.; Yin, X.; Schäferling, M.; Zhao, J.; Hein, S. M.; Braun, P. V.; Giessen, H. Large-area 3D chiral plasmonic structures. *ACS Nano* **2013**, *7*, 6321−6329.

(26) Zhang, L.; Deckhardt, E.; Weber, A.; Schönenberger, C.; Grützmacher, D. Controllable fabrication of SiGe/Si and SiGe/Si/Cr helical nanobelts. *Nanotechnology* **2005**, *16*, 655−663.

(27) Chen, W.; Bian, A.; Agarwal, A.; Liu, L.; Shen, H.; Wang, L.; Xu, C.; Kotov, N. A. Nanoparticle superstructures made by polymerase chain reaction: collective interactions of nanoparticles and a new principle for chiral materials. *Nano Lett.* **2009**, *9*, 2153−2159.

(28) Mastroianni, A. J.; Claridge, S. A.; Alivisatos, A. P. Pyramidal and chiral groupings of gold nanocrystals assembled using DNA scaffolds. *J. Am. Chem. Soc.* **2009**, *131*, 8455−8459.

(29) Yan, W.; Xu, L.; Xu, C.; Ma, W.; Kuang, H.; Wang, L.; Kotov, N. A. Self-assembly of chiral nanoparticle pyramids with strong R/S optical activity. *J. Am. Chem. Soc.* **2012**, *134*, 15114−15121.

(30) Guerrero-Martínez, A.; Auguié, B.; Alonso-Gómez, J. L.; Džolić, Z.; Gómez-Graña, S.; Žinić, M.; Cid, M. M.; Liz-Marzán, L. M. Intense optical activity from three-dimensional chiral ordering of plasmonic nanoantennas. *Angew. Chem.* **2011**, *123*, 5613−5617.

(31) Kuzyk, A.; Schreiber, R.; Fan, Z.; Pardatscher, G.; Roller, E.-M.; Högele, A.; Simmel, F. C.; Govorov, A. O.; Liedl, T. DNA-based self-assembly of chiral plasmonic nanostructures with tailored optical response. *Nature* **2012**, *483*, 311−314.

(32) Shen, X.; Song, C.; Wang, J.; Shi, D.; Wang, Z.; Liu, N.; Ding, B. Rolling up gold nanoparticle-dressed DNA origami into three-dimensional plasmonic chiral nanostructures. *J. Am. Chem. Soc.* **2012**, *134*, 146−149.

(33) Shen, X.; Asenjo-Garcia, A.; Liu, Q.; Jiang, Q.; García de Abajo, F. J.; Liu, N.; Ding, B. Three-dimensional plasmonic chiral tetramers assembled by DNA origami. *Nano Lett.* **2013**, *13*, 2128−2133.

(34) Demetriadou, A.; Pendry, J. B. Extreme chirality in Swiss roll metamaterials. *J. Phys.: Condens. Matter* **2009**, *21*, 376003.

(35) Fan, Z.; Govorov, A. O. Plasmonic circular dichroism of chiral metal nanoparticle assemblies. *Nano Lett.* **2010**, *10*, 2580−2587.

(36) Gansel, J. K.; Wegener, M.; Burger, S.; Linden, S. Gold helix photonic metamaterials: A numerical parameter study. *Opt. Express* **2010**, *18*, 1059−1069.
(37) Chigrin, D. N.; Kremers, C.; Zhukovsky, S. V. Plasmonic nanoparticle monomers and dimers: from nanoantennas to chiral metamaterials. *Appl. Phys. B: Laser Opt.* **2011**, *105*, 81−97.
(38) Zhukovsky, S. V.; Kremers, C.; Chigrin, D. N. Plasmonic rod dimers as elementary planar chiral meta-atoms. *Opt. Lett.* **2011**, *36*, 2278−2280.
(39) Zhang, S.; Zhou, J.; Park, Y.-S.; Rho, J.; Singh, R.; Nam, S.; Azad, A. K.; Chen, H.-T.; Yin, X.; Taylor, A. J.; Zhang, X. Photoinduced handedness switching in terahertz chiral metamolecules. *Nat. Commun.* **2012**, *3*, 942.
(40) Hentschel, M.; Wu, L.; Schäferling, M.; Bai, P.; Li, E. P.; Giessen, H. Optical properties of chiral three-dimensional plasmonic oligomers at the onset of charge-transfer plasmons. *ACS Nano* **2012**, *6*, 10355−10365.
(41) Eftekhari, F.; Davis, T. Strong chiral optical response from planar arrays of subwavelength metallic structures supporting surface plasmon resonances. *Phys. Rev. B* **2012**, *86*, 075428.
(42) Fan, Z.; Govorov, A. O. Chiral nanocrystals: plasmonic spectra and circular dichroism. *Nano Lett.* **2012**, *12*, 3283−3289.
(43) Hentschel, M.; Schäferling, M.; Metzger, B.; Giessen, H. Plasmonic diastereomers: adding up chiral centers. *Nano Lett.* **2013**, *13*, 600−606.
(44) Ma, W.; Kuang, H.; Wang, L.; Xu, L.; Chang, W.-S.; Zhang, H.; Sun, M.; Zhu, Y.; Zhao, Y.; Liu, L.; Xu, C.; Link, S.; Kotov, N. A. Chiral plasmonics of self-assembled nanorod dimers. *Sci. Rep.* **2013**, *3*, 1934.
(45) Yin, X.; Schäferling, M.; Metzger, B.; Giessen, H. Interpreting chiral nanophotonic spectra: the plasmonic born-kuhn model. *Nano Lett.* **2013**, *13*, 6238−6243.
(46) Govorov, A. O.; Fan, Z.; Hernandez, P.; Slocik, J. M.; Naik, R. R. Theory of circular dichroism of nanomaterials comprising chiral molecules and nanocrystals: plasmon enhancement, dipole interactions, and dielectric effects. *Nano Lett.* **2010**, *10*, 1374−1382.
(47) Govorov, A. O.; Fan, Z. Theory of chiral plasmonic nanostructures comprising metal nanocrystals and chiral molecular media. *ChemPhysChem* **2012**, *13*, 2551−2560.
(48) García-Etxarri, A.; Dionne, J. A. Surface-enhanced circular dichroism spectroscopy mediated by nonchiral nanoantennas. *Phys. Rev. B* **2013**, *87*, 235409.
(49) Zhang, H.; Govorov, A. O. Giant circular dichroism of a molecule in a region of strong plasmon resonances between two neighboring gold nanocrystals. *Phys. Rev. B* **2013**, *87*, 075410.
(50) Hendry, E.; Carpy, T.; Johnston, J.; Popland, M.; Mikhaylovskiy, R. V.; Lapthorn, A. J.; Kelly, S. M.; Barron, L. D.; Gadegaard, N.; Kadodwala, M. Ultrasensitive detection and characterization of biomolecules using superchiral fields. *Nat. Nanotechnol.* **2010**, *5*, 783−787.
(51) Gérard, V. A.; Gun'ko, Y. K.; Defrancq, E.; Govorov, A. O. Plasmon-induced CD response of oligonucleotide-conjugated metal nanoparticles. *Chem. Commun.* **2011**, *47*, 7383−7385.
(52) Slocik, J. M.; Govorov, A. O.; Naik, R. R. Plasmonic circular dichroism of peptide-functionalized gold nanoparticles. *Nano Lett.* **2011**, *11*, 701−705.
(53) Abdulrahman, N.; Fan, Z.; Tonooka, T.; Kelly, S.; Gadegaard, N.; Hendry, E.; Govorov, A. O.; Kadodwala, M. Induced chirality through electromagnetic coupling between chiral molecular layers and plasmonic nanostructures. *Nano Lett.* **2012**, *12*, 977−983.
(54) Maoz, B. M.; van der Weegen, R.; Fan, Z.; Govorov, A. O.; Ellestad, G.; Berova, N.; Meijer, E. W.; Markovich, G. Plasmonic chiroptical response of silver nanoparticles interacting with chiral supramolecular assemblies. *J. Am. Chem. Soc.* **2012**, *134*, 17807−17813.
(55) Wu, X.; Xu, L.; Liu, L.; Ma, W.; Yin, H.; Kuang, H.; Wang, L.; Xu, C.; Kotov, N. A. Unexpected chirality of nanoparticle dimers and ultrasensitive chiroplasmonic bioanalysis. *J. Am. Chem. Soc.* **2013**, *135*, 18629−18636.
(56) Ma, W.; Kuang, H.; Xu, L.; Ding, L.; Xu, C.; Wang, L.; Kotov, N. A. Attomolar DNA detection with chiral nanorod assemblies. *Nat. Commun.* **2013**, *4*, 2689.
(57) Wang, R.-Y.; Wang, P.; Liu, Y.; Zhao, W.; Zhai, D.; Hong, X.; Ji, Y.; Wu, X.; Wang, F.; Zhang, D.; Zhang, W.; Liu, R.; Zhang, X. Experimental observation of giant chiroptical amplification of small chiral molecules by gold nanosphere clusters. *J. Phys. Chem. C* **2014**, *118*, 9690−9695.
(58) Tang, Y.; Cohen, A. E. Optical chirality and its interaction with matter. *Phys. Rev. Lett.* **2010**, *104*, 163901.
(59) Choi, J. S.; Cho, M. Limitations of a superchiral field. *Phys. Rev. A* **2012**, *86*, 063834.
(60) Lipkin, D. M. Existence of a new conservation law in electromagnetic theory. *J. Math. Phys.* **1964**, *5*, 696−700.
(61) Bliokh, K.; Nori, F. Characterizing optical chirality. *Phys. Rev. A* **2011**, *83*, 021803.
(62) Coles, M. M.; Andrews, D. L. Chirality and angular momentum in optical radiation. *Phys. Rev. A* **2012**, *85*, 063810.
(63) Tang, Y.; Cohen, A. E. Enhanced enantioselectivity in excitation of chiral molecules by superchiral light. *Science* **2011**, *332*, 333−336.
(64) Rosales-Guzmán, C.; Volke-Sepulveda, K.; Torres, J. P. Light with enhanced optical chirality. *Opt. Lett.* **2012**, *37*, 3486−3488.
(65) Schäferling, M.; Dregely, D.; Hentschel, M.; Giessen, H. Tailoring enhanced optical chirality: design principles for chiral plasmonic nanostructures. *Phys. Rev. X* **2012**, *2*, 031010.
(66) Hendry, E.; Mikhaylovskiy, R. V.; Barron, L. D.; Kadodwala, M.; Davis, T. J. Chiral electromagnetic fields generated by arrays of nanoslits. *Nano Lett.* **2012**, *12*, 3640−3644.
(67) Schäferling, M.; Yin, X.; Giessen, H. Formation of chiral fields in a symmetric environment. *Opt. Express* **2012**, *20*, 26326−26336.
(68) Davis, T. J.; Hendry, E. Superchiral electromagnetic fields created by surface plasmons in nonchiral metallic nanostructures. *Phys. Rev. B* **2013**, *87*, 085405.
(69) Meinzer, N.; Hendry, E.; Barnes, W. L. Probing the chiral nature of electromagnetic fields surrounding plasmonic nanostructures. *Phys. Rev. B* **2013**, *88*, 041407.
(70) Alù, A.; Engheta, N. Theory, modeling and features of optical nanoantennas. *IEEE Trans. Antennas Propag.* **2013**, *61*, 1508−1517.
(71) Tretyakov, S.; Mariotte, F.; Simovski, C.; Kharina, T.; Heliot, J.-P. Analytical antenna model for chiral scatterers: comparison with numerical and experimental data. *IEEE Trans. Antennas Propag.* **1996**, *44*, 1006−1014.
(72) Rockstuhl, C.; Menzel, C.; Paul, T.; Lederer, F. Optical activity in chiral media composed of three-dimensional metallic meta-atoms. *Phys. Rev. B* **2009**, *79*, 035321.
(73) Yang, Z. Y.; Zhao, M.; Lu, P. X.; Lu, Y. F. Ultrabroadband optical circular polarizers consisting of double-helical nanowire structures. *Opt. Lett.* **2010**, *35*, 2588−2590.
(74) Yang, Z.; Zhao, M.; Lu, P. How to improve the signal-to-noise ratio for circular polarizers consisting of helical metamaterials? *Opt. Express* **2011**, *19*, 4255−4260.
(75) Kaschke, J.; Gansel, J. K.; Wegener, M. On metamaterial circular polarizers based on metal N-helices. *Opt. Express* **2012**, *20*, 26012−26020.
(76) Fischer, J.; Wegener, M. Three-dimensional optical laser lithography beyond the diffraction limit. *Laser Photon. Rev.* **2013**, *7*, 22−44.
(77) Sakellari, I.; Kabouraki, E.; Gray, D.; Purlys, V.; Fotakis, C.; Pikulin, A.; Bityurin, N.; Vamvakaki, M.; Farsari, M. Diffusion-assisted high-resolution direct femtosecond laser writing. *ACS Nano* **2012**, *6*, 2302−2311.
(78) Waller, E. H.; Renner, M.; von Freymann, G. Active aberration- and point-spread-function control in direct laser writing. *Opt. Express* **2012**, *20*, 24949−24956.
(79) Kern, A. M.; Martin, O. J. F. Excitation and re-emission of molecules near realistic plasmonic nanostructures. *Nano Lett.* **2011**, *11*, 482−487.
(80) Nafie, L. A. *Vibrational Optical Activity: Principles and Applications*, 1st ed.; Wiley-VCH: New York, 2011.